JOURNAL OF MATERIALS SCIENCE 33 (1998) 699–705

Characterization of zirconium, lanthanum and lead oxide deposits prepared by cathodic electrosynthesis

I. ZHITOMIRSKY, L. GAL-OR
Israel Institute of Metals, Technion-Israel Institute of Technology, Haifa, 32000, Israel

Cathodic electrosynthesis of zirconium, lanthanum and lead oxides was performed from aqueous solutions of $ZrOCl_2 \cdot 8H_2O$, $La(NO_3)_3 \cdot 6H_2O$ and $Pb(NO_3)_2$, respectively. The deposits were characterized by X-ray diffraction, thermogravimetric and differential thermal analyses. Crystallite sizes of zirconia were derived at different temperatures from X-ray broadening data. The influence of hydrogen peroxide on the electrosynthesis process, crystallization and phase evolution of deposits has been studied. A possible mechanism of electrosynthesis and the role of hydrogen peroxide are discussed. © *1998 Chapman & Hall*

1. Introduction

Electrodeposition is evolving as an important method in ceramic processing. Substantial interest exists in cathodic deposition [1–6] due to its potential in thin-film applications. Cathodic electrodeposition can be applied for the formation of various individual oxides [1–3, 6, 7], as well as for complex oxide compounds [4, 5]. In this method, a metal ion or complex is hydrolysed by electrogenerated base to form an oxide or hydroxide deposit on the cathodic substrate [1]. Hydroxide deposits can be converted to corresponding oxides by thermal treatment. Various chemical reactions which underlie the base generation in the cathodic process are discussed in the literature [1, 6].

The role of hydrogen peroxide additive in the electrodeposition process has been discussed in several works. According to Cui *et al.* [8] hydroxide deposits can be oxidized by hydrogen peroxide to form oxides. The peroxoprecursor route was designed in order to overcome problems associated with handling of titanium salts in aqueous solutions. A titanium peroxocomplex [9] is stable under certain conditions in water and can be used for the cathodic electrodeposition. It was establised that the hydrolysis of the peroxocomplex by electrogenerated base resulted in the formation of a titanium-hydrated peroxide deposit. Thermal decomposition of the deposit resulted in the formation of titania films [10, 11]. It was pointed out [10] that the hydrated peroxide films can be considered as a precursor for the preparation of corresponding oxide films.

The important finding was that complex oxide compounds can be deposited via corresponding peroxoprecursors [11–14]. Several previous investigations have been undertaken on the electrosynthesis of complex oxide compounds [11–14] via the peroxoprecursor route, including comparison of crystallization behaviour of the complex oxides with the crystallization of individual components [6, 7, 10, 11]. It was established that the obtained results correlate with those obtained in chemical precipitation experiments [15–20].

Further development of the peroxoprecursor route in electrodeposition needs better understanding of the influence of the hydrogen peroxide on the deposition process. The purpose of this work was to study the influence of hydrogen peroxide on electrodeposition of zirconium, lead and lanthanum oxides.

2. Experimental procedure

As starting materials, commercially guaranteed $ZrOCl_2 \cdot 8H_2O$ (Fluka), $Pb(NO_3)_2$ (Riedel-de Haen), $La(NO_3)_3 \cdot 6H_2O$ (Riedel-de Haen) and hydrogen peroxide (30 wt% in water) H_2O_2 (Carlo Erba) were used. Aqueous solutions of these salts were prepared and used for electrodeposition experiments. Stock solutions 1, 2 and 3 were 0.005M $ZrOCl_2$, 0.005M $La(NO_3)_3$ and 0.005M $Pb(NO_3)_2$, respectively. Also, solutions, containing various amounts of H_2O_2 additive were used. Stock solutions labelled 1H, 2H and 3H were of the same composition as 1, 2 and 3, respectively, and contained 0.1M H_2O_2 additive. Rectangular platinum specimens (40 mm × 15 mm × 0.1 mm) were used as cathodic substrates. The electrochemical cell for deposition in a galvanostatic regime included the cathodic substrate centred between two parallel platinum counterelectrodes. Cathodic deposits were obtained at a constant current density of 20 mA cm^{-2}. Deposition times were up to 15 min. After drying at room temperature deposits were removed from the substrates and subjected to X-ray diffraction (XRD) and thermogravimetric/differential thermal analysis (TG/DTA) studies. The phase content was determined by XRD with a diffractometer (Phillips, PW-1820) using monochromatized CuK_α radiation. The Scherrer relationship

$$D = \frac{0.9\lambda}{\beta \cos\theta} \quad (1)$$

was used for calculation of the crystallite size from X-ray line broadening measurements, where D is the average crystallite size, λ is the X-ray wavelength, β is the full-width at half-maximum of the peak, and θ is the Bragg angle. A commercially available computer program has been utilized for the profile-fitting procedure. Correction for instrumental broadening has been performed. The volume fraction, V_m, of the monoclinic zirconia in the samples, thermally treated at various temperatures, was calculated from peak intensities of monoclinic, I_m, and tetragonal, I_t, phases using the relationship proposed by Toraya *et al.* [21]

$$V_m = \frac{1.31X_m}{1 + 0.31X_m} \quad (2)$$

where

$$X_m = \frac{I_m(1\,1\,-1) + I_m(1\,1\,1)}{I_m(1\,1\,-1) + I_m(1\,1\,1) + I_t(1\,1\,1)}$$

Thermal analysis was carried out in air between room temperature and 900 °C at a heating rate of 10 °C min^{-1} using a computer-controlled thermoanalyser (Setaram, TGA92).

3. Results

3.1. Electrodeposition of zirconium oxides

X-ray diffractograms of fresh deposits exhibit their amorphous nature. In Fig. 1 it can be seen that deposits displayed crystalline peaks after thermal treatment at 400 °C during 1 h. For deposits obtained from solutions without hydrogen peroxide (deposits 1) the main crystalline phase at 400 °C is tetragonal zirconia. However, it is difficult to distinguish between the cubic and tetragonal zirconia phases owing to peak broadening. Faint peaks of monoclinic zirconia could also be distinguished in the X-ray diffraction pattern obtained at 400 °C. These peaks become sharper at 500 °C. At temperatures exceeding 600 °C the monoclinic phase is dominant. XRD spectra taken from deposits obtained from solution 1H (deposits 1H) show that small peaks of tetragonal and monoclinic phases appear at a treatment temperature of 400 °C. However, it should be noted that at this temperature, the specimens included a significant amount of an amorphous phase. Further increase of annealing temperature results in crystallization mainly of tetragonal zirconia, which is the main crystalline phase at 450 and 500 °C. On exposure of these deposits to higher temperatures, transformation to the monoclinic phase was observed (Fig. 1).

Fig. 2 compares the amounts of monoclinic phase found in deposits thermally treated for 1 h at different temperatures. In the temperature region of 450–550 °C the amount of monoclinic phase in deposits 1H is slightly higher than in deposits 1. However, at higher temperatures, the situation changes as the amount of monoclinic phase in deposits 1 increases more rapidly.

Table I gives experimental data on crystallite sizes of deposits 1 and 1H thermally treated at different temperatures for 1 h. As is seen from the table, the sizes of tetragonal and monoclinic crystallites are on the nanometric scale. However, the obtained powders were agglomerated. Further investigations are necessary to compare the morphologies of deposits obtained with and without hydrogen peroxide additive. It is interesting to notice that the sizes of crystallites of

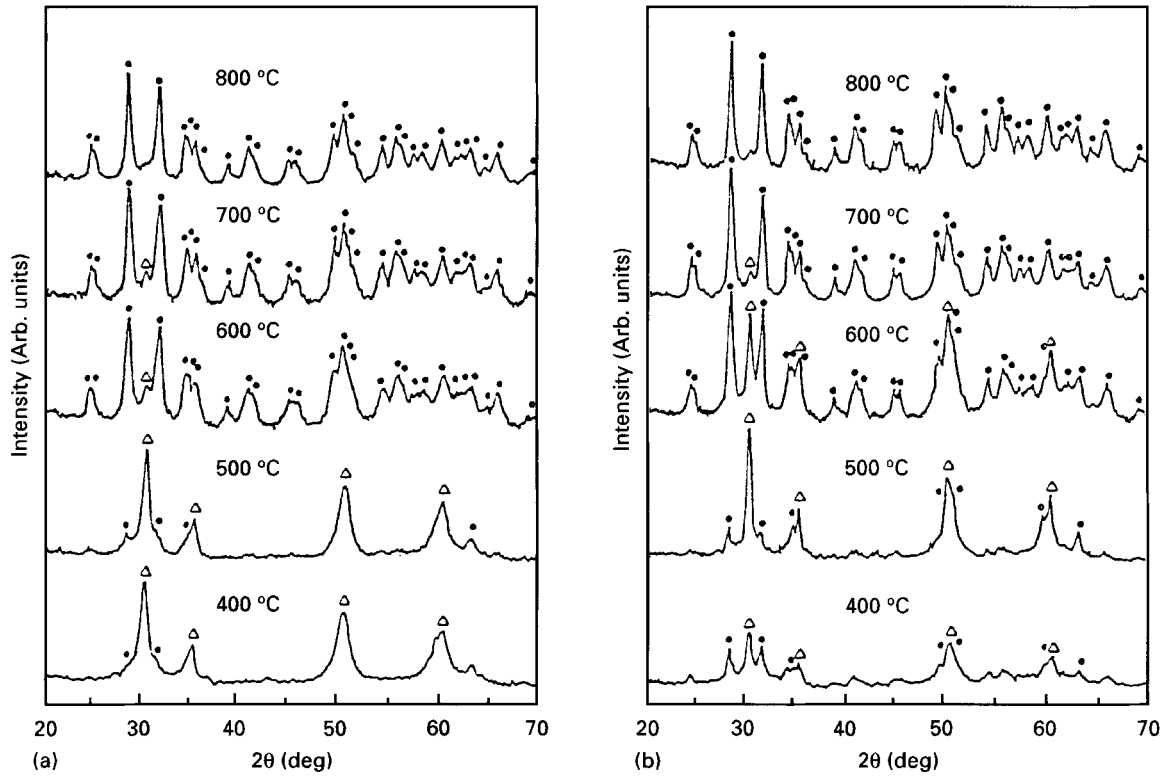

Figure 1 X-ray diffraction patterns of deposits obtained from stock solutions (a) 1 and (b) 1H, thermally treated in air at various temperatures for 1 h (△) tetragonal, (●) monoclinic zirconia.

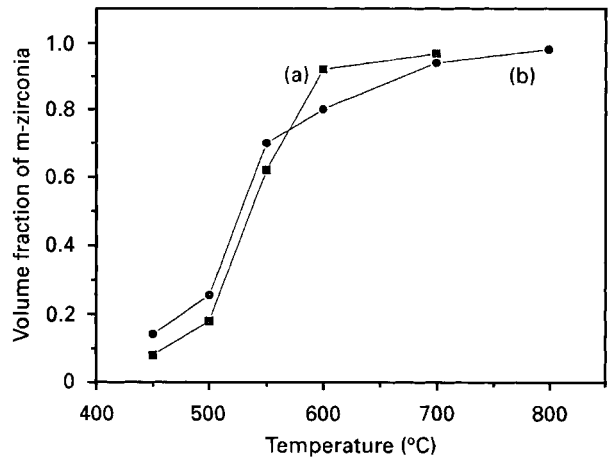

Figure 2 Volume fraction of monoclinic zirconia for deposits (a) 1 and (b) 1H thermally treated for 1 h at various temperatures.

TABLE I Crystallite sizes of zirconia phases calculated from X-ray line broadening measurements performed on deposits obtained from 0.005M $ZrOCl_2$ solutions. Reflexes used for calculations are designated

Temperature (°C)	Crystallite sizes (nm)			
	Without additive		0.1M H_2O_2 additive	
	Tetragonal (1 1 1)	Monoclinic (1 1 −1)	Tetragonal (1 1 1)	Monoclinic (1 1 −1)
400	12.1		13.5	
450	21.9		28.0	
500	19.7		26.5	
550	16.1	13.6	18.8	19.0
600		14.0		19.1
700		17.9		23.0
800		19.7		24.6
900		26.1		31.0

both tetragonal and monoclinic phase in deposits 1H are higher than the corresponding values for deposits 1. The crystallite sizes for the tetragonal phase increase when deposits 1 and 1H are heated from 400 °C to 450 °C and decrease when heated to higher temperatures. Crystallite sizes of the monoclinic phase were found to increase with the increasing temperature. However, crystallite sizes depend on the thermal treatment duration. Indeed, as seen in Fig. 3a, the crystallite size of the tetragonal phase at 450 °C decreases with time and after 15 h becomes lower than the crystallite size of the same deposits thermally treated at 500 °C for 1 h (Table I). Correspondingly, the amount of monoclinic phase increased with time as shown in Fig. 3b.

Fig. 4 shows TG/DTA curves for deposits 1 and 1H. For deposit 1, the total weight loss in the temperature region up to 900 °C is about 32.6% of the initial sample weight; however, most of the weight loss (31.2%) occurred below 400 °C. The DTA curve exhibits a broad endotherm around 125 °C and a sharp exotherm at 450 °C. For deposit 1H, two distinct steps in the TG curve are distinguished. A sharp reduction of sample weight was observed up to ~200 °C, an additional step in weight losses was recorded in the

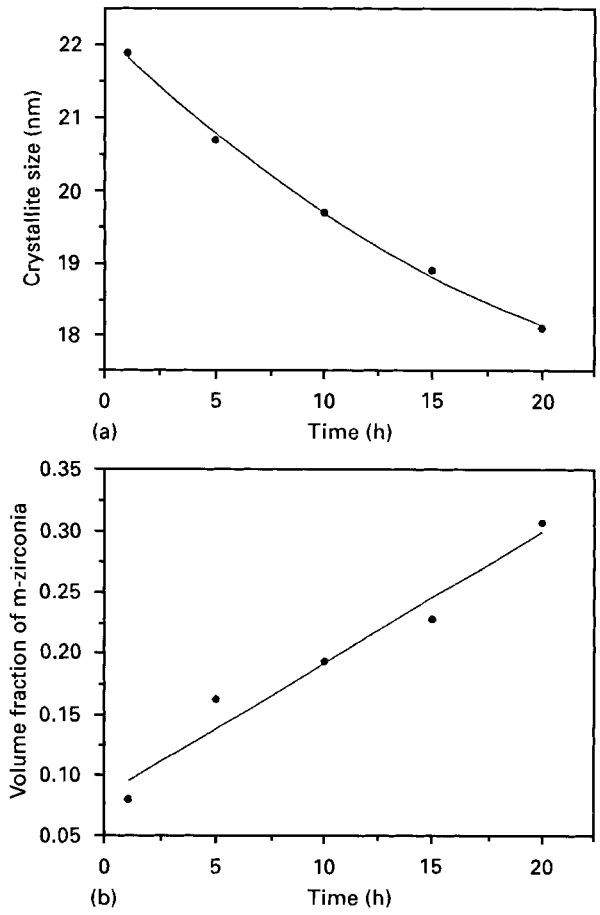

Figure 3 Crystallite size of (a) the tetragonal phase and (b) the volume fraction of the monoclinic phase for deposits 1, versus time of thermal treatment at 450 °C.

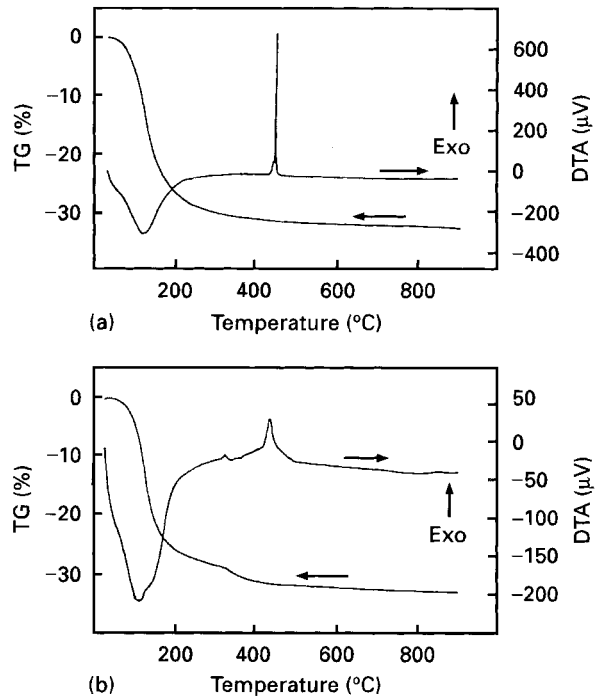

Figure 4 TG and DTA data for deposits (a) 1 and (b) 1H obtained at a 10 °C min^{-1} heating rate.

region 320–370 °C, then the weight fell gradually. Weight losses at 320 and 400 °C were 28.8% and 31.4%, respectively. The total weight loss in the temperature region up to 900 °C was 33.4%. A very broad

endothermic peak around 130 °C and an endotherm around ~450 °C are seen in the DTA curve. A small exothermic effect could also be distinguished at ~320 °C which is probably related to the above mentioned step in weight losses.

3.2. Electrodeposition of lanthanum oxides

Deposits, prepared from stock solution 2 (deposits 2) were white, whereas the deposits prepared from stock solution 2H (deposits 2H) were not purely white, but yellow tinged. The X-ray diffraction pattern of deposits 2 shows broad peaks (Fig. 5) which can be attributed to lanthanum hydroxide [22]. However, deposits were found to be amorphous, when the hydrogen peroxide concentration was 0.01 M and higher, as shown in Fig. 5.

TG records for deposits 2 and 2H shown in Fig. 6 exhibit several distinct steps in weight loss. For deposits 2, four steps were recorded: up to 200 °C, in regions 320–370 °C, 450–490 °C and finally in the region 730–810 °C. Weight losses at 260, 420 and 500 °C were 8.7%, 14.6% and 18.1%, respectively. The total weight loss at 900 °C was 28.3%. A possible link emerges between the observed endothermic effects in the DTA curve around 125, 355, 480, 790 °C and the steps in weight loss in corresponding temperature regions. A faint exothermic effect was also recorded at ~460 °C. There were three steps in weight loss for deposits 2H: below 200 °C, in the region 460–480 °C, and in the region 720–800 °C. Weight losses at 215, 490 °C were 10.1% and 20.9%, respectively, the total weight loss at 900 °C was 31.0%. Three endothermic peaks in the DTA curve at around 120, 487 and 780 °C and an exothermic peak at 479 °C were recorded for deposits 2H. It is thought that these peaks correspond to observed steps in weight losses. It should be noted that exothermic and endothermic peaks corresponding to the second step in weight losses for deposits 2H are relatively sharp. The exothermic peak for deposits 2H is more distinct than the exothermic peak for deposits 2, observed in the same temperature region. It should be pointed out that, in contrast to results obtained for deposits 2, for deposits 2H in the region 200–450 °C, weight loss changes gradually and no endothermic peak was observed.

3.3. Electrodeposition of lead oxides

X-ray diffraction patterns of dried deposits prepared from stock solution 3 (deposits 3) shows their crystalline nature (Fig. 7). The main peaks can be attributed to β-PbO (yellow), as the observed *d*-spacings correlated closely with the JCPDS card [23]. However, a difference in the relative intensities of the peaks was

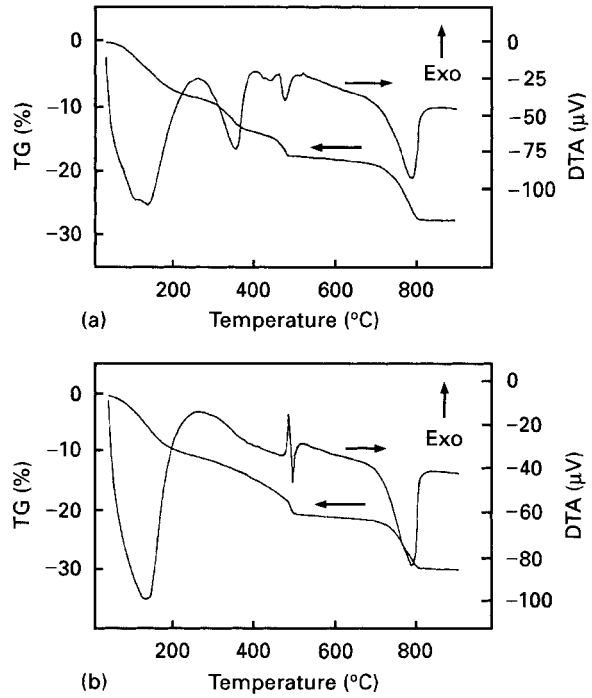

Figure 6 TG and DTA data for deposits (a) 2 and (b) 2H obtained at a 10 °C min^{-1} heating rate.

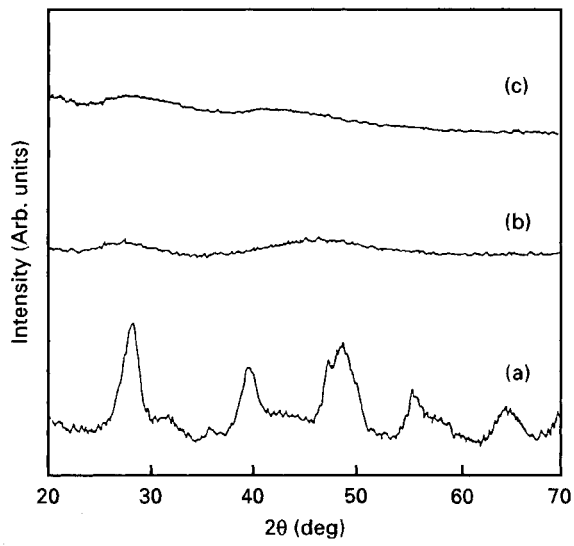

Figure 5 X-ray diffraction patterns of deposits obtained from 0.005 M $La(NO_3)_3$ solution: (a) without additive, (b) 0.01 M H_2O_2 additive and (c) 0.1 M H_2O_2 additive.

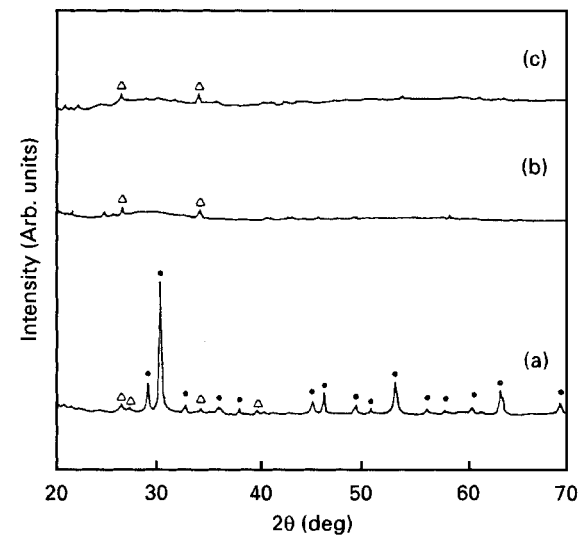

Figure 7 X-ray diffraction patterns of deposits obtained from 0.005 M $Pb(NO_3)_2$ solution: (a) without additive, (b) 0.01 M H_2O_2 additive and (c) 0.1 M H_2O_2 additive; (●) PbO, (△) $2PbCO_3 \cdot Pb(OH)_2$.

observed when compared to the JCPDS file [23], and also in the X-ray intensities obtained in experiments performed with graphite substrates [7]. In addition to peaks of β-PbO, the diffractograms also showed small peaks of $2PbCO_3 \cdot Pb(OH)_2$. Deposits were crystalline when the hydrogen peroxide concentration was 0.005M and exhibited an amorphous nature when concentration of the additive was 0.01M and higher, as it is shown in Fig. 7. Faint peaks of $2PbCO_3 \cdot Pb(OH)_2$ could also be distinguished in X-ray diffraction patterns of deposits obtained from solution 3H (deposits 3H). Deposits 3H were reddish yellow and in contrast to deposits 3 they were well adherent to the substrate.

4. Discussion

4.1. Zirconium oxide deposits

In the electrosynthesis method, the high pH of the cathodic region brings about formation of colloidal particles, which precipitate on the electrode. The possible cathodic reaction that generates OH^- is

$$2H_2O + 2e^- \rightleftharpoons H_2 + 2OH^- \quad (3)$$

The following anodic reaction is supposed to occur simultaneously

$$2H_2O \rightleftharpoons O_2 + 4H^+ + 4e^- \quad (4)$$

Owing to the complex chemistry of zirconium species in aqueous solutions [24–28], difficulties are encountered in identification of the scheme for reactions which underly the deposition process. According to various authors [24–28], various polynuclear positively charged species exist in the solutions; however, in zirconyl chloride solutions, tetramers $[Zr_4(OH)_8(H_2O)_{16}]^{8+}$ can be considered as a main zirconium species [24, 25]. Following the scheme proposed by Blesa *et al.* [24], it can be assumed that the tetramers are hydrolysed by electrogenerated base to form a $Zr_4O_{8-x}(OH)_{2x}$ deposit. Thermal treatment results in dehydration [26] of $Zr_4O_{8-x}(OH)_{2x}$ to form ZrO_2. However, when deposition is performed in the presence of hydrogen peroxide, the formation of the hydrated zirconium peroxide $ZrO(O_2)(H_2O)_x$ can be expected [20, 29]. The hydrated zirconium peroxide is further decomposed with liberation of water and oxygen to form ZrO_2

$$2ZrO(O_2)(H_2O)_x \rightarrow 2\,ZrO_2 + O_2 + 2xH_2O \quad (5)$$

As seen from Fig. 1 the main crystalline phase in the region 400–500 °C is tetragonal zirconia. The particle-size distribution of the tetragonal phase is influenced by the calcination temperature and kinetics of transformation to the monoclinic phase. The increase in particle size of the tetragonal phase for deposits 1 and deposits 1H, observed when heating from 400 °C to 450 °C is attributed to an increase of temperature. However, the size of tetragonal crystallites exceeds the critical value of about 10 nm [30], and as a result, transformation to the monoclinic phase is observed. The crystallite size of the monoclinic phase at 550 °C is lower than that of the tetragonal phase at 450 and 500 °C. This is in agreement with experimental results reported elsewhere [11, 26, 31], according to which the crystallite sizes of the monoclinic phase were found to be lower than those of the tetragonal phase from which they were derived. However, it was established that the crystallite size of the tetragonal phase (Table I) decreased at temperatures higher than 450 °C. This result can be understood when kinetic factors [32] are taken into consideration. According to Mercera *et al.* [31] transformation from the tetragonal to the monoclinic phase brings about changes in crystallite size distribution. When tetragonal crystallites exceeding a critical size are converted to monoclinic, the transformation process excludes larger crystallites from the distribution, as a result the average crystallite size of the tetragonal phase decreases. Turning again to experimental results shown in Fig. 3, it is seen that the particle size of the tetragonal phase and the amount of monoclinic phase depend to a great extent on calcination duration. After prolonged calcination at 450 °C the average particle size of the tetragonal phase becomes lower than that observed at 500 °C.

The obtained results exhibited differences in X-ray data for deposits 1 and 1H. As seen from Fig. 1 at 400 °C, deposits 1 show well-defined peaks of the tetragonal phase, whereas peaks of the monoclinic phase are slight. In contrast, at this temperature deposits 1H contained a significant amount of amorphous phase, and the X-ray diffraction pattern at 400 °C shows relatively slight peaks of tetragonal and monoclinic phases. Experimental results presented in Figs 1 and 2 indicate that, in the case of deposits 1H, crystallization from the amorphous phase starts at a higher temperature and the temperature interval of transformation from tetragonal to monoclinic phase is relatively broad as compared to those for deposits 1. As pointed out above, the crystallite sizes of deposits 1H for both tetragonal and monoclinic phases are higher than the corresponding values for deposits 1 in all studied temperature intervals.

Thermal analysis revealed weight losses for deposits 1 and 1H which are attributed to a gradual decomposition of green deposits to form zirconia (Fig. 4). For deposits 1H, weight loss occurs in two steps. Similar steps were observed for zirconia deposits prepared from mixed water–methyl alcohol solutions in the presence of hydrogen peroxide [11]. The observed endothermic peaks are associated with the weight losses. The exothermic peaks at around 450 °C are considered to be due to crystallization of zirconia phases and are in agreement with the X-ray data. The exothermic peak for deposits 1H is very broad compared to that for deposits 1. It can be summarized that, in experiments on zirconia electrodeposition performed with and without hydrogen peroxide, differences were observed in TG–DTA data, X-ray data on crystallization and evolution of phases with temperature and sizes of crystallites.

4.2. Lanthanum oxide deposits

La^{3+} ions are highly hydrolysed in aqueous solutions and form various polynucleus species [33]. According to Chanaud *et al.* [33] and Suzuki *et al.* [34], hydroxide precipitation commences at pH ~7.5 and is

complete at pH ~10. However, owing to the existence of $[La(OH)_4]^-$ species, the hydroxide is slightly soluble at higher pH [33]. It is supposed that in electrodeposition experiments, the high pH near the cathode brings about the formation of hydroxide $La_q(OH)_{3q}(OH_2)_y$ [33]. However, deposits 2 and 2H exhibited differences in colour, crystallinity and TG–DTA data. It should be noted that, in contrast to results described in this work, no influence of hydrogen peroxide on the precipitation of lanthanum component was detected by Blesa *et al.* [20].

4.3. Lead oxide deposits

The crystallinity of the deposit obtained from solution 3 is in agreement with previous experiments performed on graphite substrates. The appearance of the $2PbCO_3 \cdot Pb(OH)_2$ phase could be attributed to a reaction with CO_2 during drying in air. However, the addition of hydrogen peroxide brings about the formation of amorphous deposits. In addition, differences in colour and adhesion of the deposits were observed. It is important to note that results obtained in the $Pb(NO_3)_2$–NH_4OH–H_2O_2 system [16, 20] show that the crystalline lead hydroxide precipitate was found to be oxidized by hydrogen peroxide to form amorphous $3PbO \cdot 2PbO_2 \cdot 3H_2O$. A coloration effect of the hydrogen peroxide additive on green precipitates was also observed [20].

4.4. Electrodeposition via hydroxide or peroxide precursors

The formation of oxide materials via corresponding hydroxides or peroxides constitute two different chemical routes in electrosynthesis. The differences encompass chemical species in starting solutions, conditions of precipitation and composition of precipitates, their crystallinity and phase evolution with temperature. The possibility to obtain stable species in solution, as well as to achieve conditions for their precipitation at the cathode [10], is of paramount importance for electrosynthesis. In the case of electrosynthesis of complex oxide compounds, conditions for cathodic coprecipitation have to be achieved [11–14]. Previous experiments have shown the importance of the peroxoprecursor route, which provides additional possibilities in electrodeposition of various materials. This approach allowed the problem of titania deposition to be solved and experimental conditions for the formation of complex compounds such as $ZrTiO_4$ and PZT (lead zirconate titanate) to be found via cathodic precipitation of corresponding peroxoprecursors [10–14]. Results of this work, coupled with previous results [7, 10–14], pave the way for electrodeposition of PLZT (lead lanthanum zirconate titanate) solid solutions.

5. Conclusion

Zirconium, lanthanum and lead oxide deposits were obtained from aqueous solutions of $ZrOCl_2 \cdot 8H_2O$, $La(NO_3)_3 \cdot 6H_2O$ and $Pb(NO_3)_2$, respectively via the cathodic electrosynthesis method, and experimental results obtained with and without hydrogen peroxide were compared. It can be summarized that in experiments on zirconia electrodeposition performed with and without hydrogen peroxide, differences were observed in TG–DTA data, X-ray data on crystallization, evolution of obtained phases with temperature, and sizes of crystallites. Hydrogen peroxide was found to exert an influence also on the composition and properties of deposits obtained from lead and lanthanum nitrate solutions, as indicated by formation of amorphous deposits instead of crystalline deposits deposited in the absence of H_2O_2. Differences in TG/DTA data for lanthanum-containing deposits 2 and 2 H were also observed. The results of this work, coupled with previous results, indicate that electrodeposition of various oxides can be achieved via hydroxide or peroxide precursors. Further development of the peroxide route will allow new possibilities in electrodeposition.

References

1. J. A. SWITZER, *Am. Ceram. Soc. Bull.* **66** (1987) 1521.
2. D. TENCH and L. F. WARREN, *J. Electrochem. Soc.* **130** (1983) 869.
3. P. M. S. MONK, S. L. CHESTER, D. S. HIGHAM and R. D. PARTRIDGE, *Electrochim. Acta* **39** (1994) 2277.
4. S. B. ABOLMAALI and J. B. TALBOT, *J. Electrochem. Soc.* **140** (1993) 443.
5. P. SLEZAK and A. WIECKOWSKI, *ibid.* **138** (1991) 1038.
6. L. GAL-OR, I. SILBERMAN and R. CHAIM, *ibid.* **138** (1991) 1939.
7. I. ZHITOMIRSKY, L. GAL-OR, A. KOHN and H. W. HENNICKE, *J. Mater. Sci. Lett.* **14** (1995) 807.
8. C. Q. CUI, S. P. JIANG and A. C. C. TSEUNG, *J. Electrochem. Soc.* **139** (1992) 60.
9. J. MUHLEBACH, K. MULLER and G. SCHWARZENBACH, *Inorg. Chem.* **9** (1970) 2381.
10. I. ZHITOMIRSKY, L. GAL-OR, A. KOHN and H. W. HENNICKE, *J. Mater. Sci.* **30** (1995) 5307.
11. I. ZHITOMIRSKY and L. GAL-OR, *J. Eur. Ceram. Soc.* **16** (1996) 819.
12. I. ZHITOMIRSKY, L. GAL-OR and S. KLEIN, *J. Mater. Sci. Lett.* **14** (1995) 60.
13. I. ZHITOMIRSKY, L. GAL-OR and A. KOHN, *Mater. Lett.* **25** (1995) 223.
14. I. ZHITOMIRSKY, L. GAL-OR, A. KOHN and M. D. SPANG, *J. Mater. Sci.* **32** (1997) 803.
15. J. A. NAVIO, F. J. MARCHENA, M. MACIAS, P. J. SANCHEZ-SOTO and P. PICHAT, *ibid.* **27** (1992) 2463.
16. M. MURATA, K. WAKINO, K. TANAKA and Y. HAMAKAWA, *Mater. Res. Bull.* **11** (1976) 323.
17. G. PFAFF, *Z. Chem.* **28** (1988) 76.
18. G. PFAFF, *J. Eur. Ceram. Soc.* **12** (1993) 159.
19. J. A. NAVIO, M. MACIAS and P. J. SANCHEZ-SOTO, *J. Mater. Sci. Lett.* **11** (1992) 1570.
20. Y. YOSHIKAWA and K. TSUZUKI, *J. Eur. Ceram. Soc.* **6** (1990) 227.
21. H. TORAYA, M. YOSHIMURA and S. SOMIYA, *J. Am. Ceram. Soc.* **67** (1984) C-119.
22. JCPDS Index Card 36-1481 (Joint Committee for Powder Diffraction Studies, Swarthmore, PA, 1990).
23. JCPDS Index Card 38-1477 (Joint Committee for Powder Diffraction Studies, Swarthmore, PA, 1988).
24. M. A. BLESA, A. J. G. MAROTO, S. I. PASSAGGIO, N. E. FIGLIOLIA and G. RIGOTTI, *J. Mater. Sci.* **20** (1985) 4601.
25. A. CLEARFIELD, *J. Mater. Res.* **5** (1990) 161.
26. R. SRINIVASAN, M. B. HARRIS, S. F. SIMPSON, R. J. DE ANGELIS and B. H. DAVIS, *ibid.* **3** (1988) 787.

27. W. ZHANG and F. P. GLASSER, *J. Mater. Sci.* **28** (1993) 1129.
28. J.-H. CHOY, Y.-S. HAN and J.-T. KIM, *Mater. Chem.* **5** (1995) 65.
29. R. J. H. CLARK, D. C. BRADLEY, P. THORNTON, "The Chemistry of Titanium, Zirconium and Hafnium" (Pergamon Press, Oxford, New York, Toronto, 1975) p. 453.
30. R. C. GARVIE and M. F. GOSS, *J. Mater. Sci.* **21** (1986) 1257.
31. P. D. L. MERCERA, J. G. VAN OMMEN, E. B. M. DOESBURG, A. J. BURGGRAAF and J. R. H. ROSS, *Appl. Catal.* **57** (1990) 127.
32. *Idem., J. Mater. Sci.* **27** (1992) 4890.
33. R. CHANAUD, A. JULBE, P. VAIJA, M. PERSIN and L. COT, *J. Mater. Sci.* **29** (1994) 4244.
34. Y. SUZUKI, H. SAITON, Y. KAMATA, Y. AIHARA and Y. TATEYAMA, *J. Less-Common Metals* **149** (1989) 179.

Received 5 September 1996
and accepted 22 August 1997